Bioactive Materials 10 (2022) 367–377

Contents lists available at ScienceDirect

Bioactive Materials

journal homepage: www.sciencedirect.com/journal/bioactive-materials

Profiling the responsiveness of focal adhesions of human cardiomyocytes to extracellular dynamic nano-topography

Huaiyu Shi [a,b], Xiangjun Wu [a,b], Shiyang Sun [a,b], Chenyan Wang [a,b], Zacharias Vangelatos [c], Ariel Ash-Shakoor [a], Costas P. Grigoropoulos [c], Patrick T. Mather [d], James H. Henderson [a,b], Zhen Ma [a,b,*]

[a] Department of Biomedical & Chemical Engineering, Syracuse University, Syracuse, NY, 13244, USA
[b] BioInspired Syracuse Institute for Materials and Living Systems, Syracuse University, Syracuse, NY, 13244, USA
[c] Department of Mechanical Engineering, University of California, Berkeley, PA, 94720, USA
[d] Department of Chemical Engineering, Bucknell University, Lewisburg, PA, 17837, USA

ARTICLE INFO

Keywords:
Stimuli-responsive biomaterials
Shape memory polymer
Focal adhesion
Costamere
Dynamic mechanobiology
Human induced pluripotent stem cells

ABSTRACT

Focal adhesion complexes function as the mediators of cell-extracellular matrix interactions to sense and transmit the extracellular signals. Previous studies have demonstrated that cardiomyocyte focal adhesions can be modulated by surface topographic features. However, the response of focal adhesions to dynamic surface topographic changes remains underexplored. To study this dynamic responsiveness of focal adhesions, we utilized a shape memory polymer-based substrate that can produce a flat-to-wrinkle surface transition triggered by an increase of temperature. Using this dynamic culture system, we analyzed three proteins (paxillin, vinculin and zyxin) from different layers of the focal adhesion complex in response to dynamic extracellular topographic change. Hence, we quantified the dynamic profile of cardiomyocyte focal adhesion in a time-dependent manner, which provides new understanding of dynamic cardiac mechanobiology.

1. Introduction

After decades of endeavor, many studies have demonstrated that extracellular matrix (**ECM**) plays a key role in biophysical regulation of cellular morphology, differentiation, and maturation [1–3]. Though a variety of cell culture systems have been established to recapitulate the complexity of natural ECM, current static platforms are not able to investigate cell responsiveness to the ECM that is consistently changing during tissue development and disease progression. Many approaches have been pursued to provide dynamic cues to cell culture systems [4–6]. Particularly, stimuli-responsive biomaterials are used to create cell culture substrates with dynamic mechanical features, which enable the study of how a changing extracellular microenvironment mediates cellular development [7–9]. As a class of stimuli-responsive biomaterials, shape memory polymers (**SMP**) can recover from a temporary programmed shape to their permanent shape in response to different external stimuli [10,11]. In particularly applications of SMP, dynamic topography has been achieved to study cell mechanobiological responsiveness during temporal-specific cell-matrix interactions [12–14].

Cell-matrix interactions are primarily sensed and transduced through focal adhesions to regulate cell behaviors and functions [15–19]. The focal adhesion complexes are composed of a three-layer architecture: the outermost signaling layer, containing integrins, focal adhesion kinase (**FAK**) and paxillin, links cell membrane to the ECM; the innermost layer, containing α-actinin, zyxin and vasodilator-stimulated phosphoprotein, binds to cytoskeletal actin filaments; and the intermediate layer, containing vinculin and talin, transduces force from integrins to the actin filaments [20]. It has been well documented that nanoscale surface topography affects focal adhesion protein synthesis, assembly, maturation, and disassembly, which eventually regulate cell shape, spreading, migration and differentiation [21–23]. Particularly for cardiomyocytes, biocompatible substrates with different topographic features have been shown to affect the expression, distribution, and orientation of focal adhesions to further enhance cardiomyocyte alignment and contractility [24–27]. However, these studies are still built based on the static systems and unable to probe focal adhesion dynamics

Peer review under responsibility of KeAi Communications Co., Ltd.
* Corresponding author. Department of Biomedical & Chemical Engineering, Syracuse University, Syracuse, NY, 13244, USA.
E-mail address: zma112@syr.edu (Z. Ma).

https://doi.org/10.1016/j.bioactmat.2021.08.028
Received 12 April 2021; Received in revised form 17 July 2021; Accepted 25 August 2021
Available online 28 August 2021

Abbreviations

ECM	extracellular matrix
SMP	shape memory polymer
FAK	focal adhesion kinase
***t*BA**	*tert*-butyl acrylate
BA	butyl acrylate
hiPSC-CMs	human induced pluripotent stem cells-derived cardiomyocytes
pFAs	peripheral focal adhesions
PEM	polyelectrolyte multilayer
PEI	polyethylenimine
PSS	poly(styrene 4-sulfonate)
PAA	poly(allylamine hydrochloride)
tFA	total focal adhesion
AFM	atomic force microscopy

in vitro.

Using biocompatible programmable platforms, researchers focus on how dynamic signals would impact cell adhesion properties [28]. For example, by applying biaxial mechanical stretching to human mesenchymal stem cells, the total number of focal adhesions was significantly increased, which further reduced the adipogenesis potential [29]. In another study, mechanical stretching was able to induce the sliding of focal adhesions during cellular reorganization, instead of formation of focal adhesions *de novo* [30]. Compared to many traditional means of mechanically applying external stimulation, stimuli-responsive materials can reproduce gradual and reversible changes in their mechanical properties in response to environmental triggers. For example, a magnetic-responsive PDMS-based substrate was fabricated to apply dynamic forces to fibroblasts, and focal adhesions were assembled at the regions experiencing the forces [7]. A hyaluronic acid-collagen hydrogel with deformation-induced exchangeable hydrazone crosslinking has been reported to be able to promote the recruitment of paxillin and β1-integrin, indicating enhanced focal adhesion assembly in response to the dynamic mechanical cues from the microenvironment induced by stress relaxation of viscoelastic hydrogel [31]. A polycaprolactone SMP-based cell culture substrate was fabricated with dynamic surface topography, which could be changed in the orthogonal direction. Using this dynamic substrate, focal adhesions of cardiomyocytes derived from neonatal rats could be reoriented with surface topographic change during shape transition [32]. In our previous study, employing *tert*-butyl acrylate (***t*BA**) and butyl acrylate (**BA**) copolymer, we established a cytocompatible substrate with a dynamic flat-to-wrinkle nano-topographic surface. We demonstrated the progressive myofibril reorganization and morphological alignment of cardiomyocytes derived from human induced pluripotent stem cells (**hiPSC-CMs**) in response to the dynamic topographic change [33]. However, how focal adhesions of human cardiomyocytes respond to dynamic extracellular topographic changes has not yet been documented.

In this study, we combined a SMP-based dynamic cell culture substrate and human induced pluripotent stem cell (**hiPSC**) technology to study the dynamic responses of focal adhesions of hiPSC-CMs to a changing extracellular mechanical microenvironment. Three focal adhesion proteins (paxillin, vinculin and zyxin) were investigated to track the dynamic changes of different layers of focal adhesion complexes. We found that peripheral focal adhesions (**pFAs**), the focal adhesions near the cell edge, were reoriented with the direction of dynamic nano-wrinkle formation. Upon flat-to-wrinkled transition from the SMP-based substrate, we profiled a sequential series of focal adhesion responsiveness to a dynamic nano-topographic surface. Moreover, we quantified the dynamic behaviors of costameres, the striated muscle-specific focal adhesions, which play an important role of transmitting cardiac contraction force from sarcomeres to ECM. This study would provide detailed evidence to fill in the knowledge gap of how cardiomyocytes receive extracellular mechanical inputs to initiate intracellular myofibril alignment, which could make significant progress in understanding the process of cardiomyocyte maturation *in vitro*.

2. Materials and methods

2.1. SMP fabrication and polyelectrolyte multilayer (PEM) coating

The SMPs were fabricated by UV polymerization of four components: monomers acrylic acid *tert*-butyl ester (***t*BA**) (AcRos Organics, Ca#371130010) and acrylic acid butyl ester (**BA**) (Sigma-Aldrich, Ca# 234923); crosslinker, 3,6,9-trioxaundecamethylene dimethacrylate (Sigma Aldrich, Ca# 86680); and photoinitiator, benzil α, α-dimethyl acetal (Sigma Aldrich, Ca#196118). The monomer solution containing 95 wt% *t*BA and 5 wt% BA was prepared by mixing with 5 wt% crosslinker and 1 wt% photoinitiator [34]. The SMP samples were polymerized in a UV box (Black Ray, 365 nm, 2.0 mW/cm^2). After 1-h crosslinking, samples were immersed in a 50% methanol aqueous solution for 6 h to rinse the excess monomers. Next, rinsed SMPs were settled under a chemical hood for 24 h to remove moisture and further dehydrated under −15 PSI in a vacuum oven at 40 °C for additional 24 h. Dried samples were cut into 25 mm × 5 mm rectangles and uniaxially stretched to 140% of their original length under 65 °C to program strained temporal shape.

To enable the dynamic nano-wrinkle formation during SMP shape recovery, stretched SMPs were coated with PEM thin film. To prepare the PEM coating, polyethylenimine (**PEI**) (Sigma, Ca# 408727) was prepared as a 3 wt% PEI solution. The solutions of poly(sodium 4-styrenesulfonate) (**PSS**) (Sigma Aldrich, Ca# 434574) and poly(allylamine hydrochloride) (**PAA**) (Sigma Aldrich, Ca# 283215) were prepared with final concentration at 0.1 M and pH at ~3.5 using halite (Sigma Aldrich, Ca# 57653). The SMP with 40% strain adhered onto a glass slide vacuumed on the spin coater for PEM coating. The PEM coating is initialized with one layer of PEI solution. Next, 20 bilayers of polyanion (PSS) and polycation (PAA), with twice water purging between each coating, were successively spin-coated on the SMP surface at 3000 rpm for 12 s (Fig. 1 a) [34].

2.2. hiPSC-CMs preparation and seeding

hiPSCs were passaged every 3 days with seeding density of 2.5 × 10^4 cells/cm^2 in a Geltrex-coated 6-well plate (Thermo Fisher Scientific, Ca# A1413302) and maintained in the Essential 8 media (Thermo Fisher Scientific, Ca# A1517001). The hiPSC-CM differentiation was carried out as previously described [35]. Briefly, two molecules, GSK3 inhibitor (6 μM, CHIR99021; Stemgent, Ca# 04-0004) and WNT inhibitor (5 μM, IWP4; Stemgent, Ca# 04–0036), were used to regulate the WNT pathway for hiPSC-CM differentiation. The differentiated hiPSC-CMs were cultured in RPMI-1640 media (Thermo Fisher Scientific, Ca# A1517001) with B27 complete supplement (Thermo Fisher Scientific, Ca# 17504044) (**RPMI-B27-C**) until Day 20. Next, the hiPSC-CMs were disassociated and cultured in DMEM no glucose media with 4 mM lactate, GlutaMAX (Thermo Fisher Scientific, Ca# 35050061) and NEAA (Thermo Fisher Scientific, Ca# 11140050) for a 6-day purification. SMP-PEM substrates were sterilized in a biosafety cabinet under UV radiation for 30 min for each side. Sterilized SMP-PEM substrates were put in a 48-well plate and coated with Geltrex overnight under room temperature. 3 × 10^4 purified hiPSC-CMs were seeded per polymer substrate and incubated at 30 °C with 5% CO_2 for two days, before transferring the plate into a 37 °C incubator.

2.3. Substrate characterization

Atomic force microscopy (**AFM**) scanning was performed to

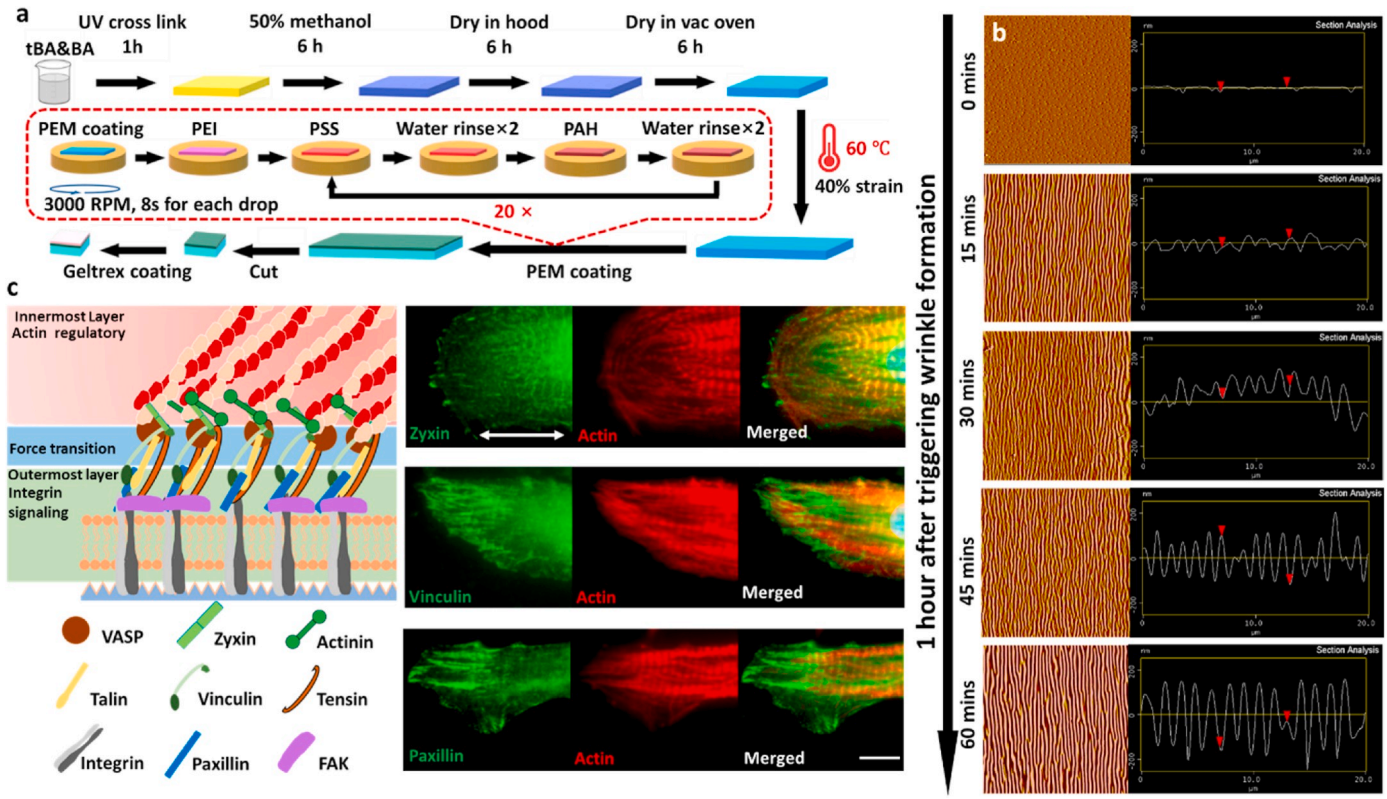

Fig. 1. Programmable SMP-PEM substrate for study of hiPSC-CMs' focal adhesions. (a) Schematics showing the fabrication of SMP-PEM substrate for cell seeding. (b) AFM images showing the dynamic nano-wrinkle formation on Geltrex-coated SMP-PEM surface at 0, 15, 30, 45, and 60 min post temperature increase in a hydrated condition. (c) Schematic of focal adhesion complex and confocal images showing hiPSC-CM focal adhesions on nano-wrinkled surface, including paxillin, vinculin and zyxin together with F-actin (scale bar: 8 μm). Arrow indicate the wrinkle direction.

characterize the dynamic topography of SMP-PEM substrate during flat-to-wrinkle transition after triggering the shape recovery in a liquid environment. The strained SMP-PEM substrate used for AFM characterization was coated with Geltrex overnight at room temperature, washed with RPMI-B27-C media, and then transferred to 37 °C for triggering shape recovery with the temperature switching. For the next 60 min, SMP-PEM samples were collected every 15 min. AFM (Nano R-2 from Pacific Nanotechnology), under 2 Hz scanning frequency, was then carried out using a Si_3N_4 cantilever (Spring constant: 5 N/m) to scan a 2500 μm^2 square area to probe the topographic feature of SMP during dynamic transition.

To evaluate the surface stiffness of the polymer substates, micro-indentation experiments were conducted using the Hysitron PI 88 SEM PicoIndenter mounted inside the chamber of a scanning electron microscope (FEI Quanta 3D FEG) to enable high precision nano-mechanical testing. Three different substrates were used in this study, including SMP without PEM coating (SMP only), Flat (unstrained flat SMP-PEM) and Winkled (pre-recovered wrinkled SMP-PEM). The substrates were attached to the SEM pin stub mounts (TED PELLA) with PELCO® Pro C100 Cyanoacrylate Glue, TED PELLA). For the indentation experiments, a flat end cylindrical punch (Hysitron TI-0145 Flat ended, 60°, 10 μm diameter) was used. The maximum force was set equal to 300 μN and maximum displacement 30 nm with 10 nm/s loading rate. To determine the modulus, the slope of the force-displacement relationship curve S was measured at the beginning of the unloading [36]. To improve the precision of the slope measurement, the noise from the data was filtered. To calculate the Young's Modulus, the standard methodology of Oliver and Pharr was used, leading to $E = S/2a$, where a is the diameter of the flat punch [37].

2.4. Immunocytochemistry

To perform immunocytochemistry, cell samples were fixed by 4% PFA solution for 20 min. After three times of PBS washing, the samples were immersed in 0.2% Triton (Sigma Aldrich, Ca# T8787) for 5 min for permeabilization and then treated with bovine serum albumin (BSA; Sigma Aldrich, Ca# A8022) for 30 min for blocking. The fixed samples were then incubated with primary antibody solution (Table S1) for 2 h and then secondary antibodies for another 2 h. After three times of PBS washing to purge the unlinked primary antibody, the samples were immersed in DAPI to stain the nuclei. The bright-field and epifluorescence microscopy was performed on a Nikon Eclipse Ti microscope with a Zyla 4.2 PLUS sCMOS camera. The confocal microscopy was performed on a Zeiss LSM 710 confocal microscope.

2.5. Quantification of focal adhesion properties

The analyses of pFAs were performed using fluorescent images of the focal adhesion proteins (zyxin, vinculin and paxillin) from individual hiPSC-CMs. The orientation of pFAs was measured based on the angle between wrinkle direction and staining of focal adhesions close to the cell periphery. For the flat surface, orientation was measured based on the angle between staining of focal adhesions and X-axis of the image. The length of pFA was measured based on the staining of focal adhesions at the cell periphery. To analyze the expression of pFA, epifluorescence microscopy was set at the same exposure (200 ms, 80% solar intensity). Next, fluorescent intensity was measured using a square box (9 × 9, 81 pixels, 0.91 μm^2) on the pFAs, and then normalized to the intensity value of fluorescent background from the regions without cell or debris.

The analyses of costameres were performed based on the fluorescent images of the focal adhesion proteins (zyxin, vinculin and paxillin)

together with actin myofibrils, which were binarized by applying an intensity threshold (Fig. S1). Total number of focal adhesions within individual hiPSC-CMs was measured based on the particle analysis of binarized images of focal adhesions using ImageJ. Sarcomere number was measured based on the particle analysis of binarized images of actin. Costamere number was measured based on the colocalization of focal adhesions and actin. Cell area was measured using ImageJ. The parameters of costamere density, total focal adhesion (**tFA**) density, ratio of costamere to total focal adhesion (costamere-tFA ratio) and ratio of costamere to sarcomere (costamere-sarcomere ratio) were calculated as follow:

$$Costamere\ density = \frac{\text{Costamere number(count)}}{\text{Cell area}(\mu m^2)}$$

$$Total\ focal\ adhesion\ density = \frac{\text{Total focal adhesion number(count)}}{\text{Cell area}(\mu m^2)}$$

$$Ratio\ of\ costamere\ to\ total\ focal\ adhesion = \frac{\text{Costamere density}}{\text{Total focal adhesion density}}$$

$$Ratio\ of\ costamere\ to\ sarcomere = \frac{\text{Costamere number}}{\text{Sarcomere number}}$$

2.6. Contractile function analysis

Contractile function analysis of individual hiPSC-CMs was performed using an open-source motion-tracking software, which can be reached at https://gladstone.org/46749d811. The video of hiPSC-CM beating was imported to the software and analyzed to output the parameters of beat rate (beating per minute), time interval between contraction and relaxation (C-R interval), contraction velocity (μm per second), relaxation velocity (μm per second) and X/Y contraction ratio (X-direction contraction velocity divided by Y-direction contraction velocity).

2.7. Statistical analysis

One-way ANOVA with Tukey multiple *t*-test was used to compare the difference among groups. The statistical significance was determined as *p*-value < 0.05 (*), <0.01(**), <0.001 (***) and <0.0001 (****), respectively. For each condition, more than 20 hiPSC-CMs were selected for quantification. In length measurement and orientation analysis, all clear elongated pFAs within each hiPSC-CM were measured for every condition. In focal adhesion expression analysis, each hiPSC-CM was randomly selected 6 different locations for fluorescent intensity measurement. Data visualization, including the violin plot and polar histogram, was carried out using OriginLab.

3. Results

3.1. Nano-wrinkle formation on SMP-PEM surface

The fabricated SMP-PEM substrate was cut into appropriate size for seeding of hiPSC-CMs (Fig. 1 a). The SMPs are able to maintain the strain under 30 °C and return to the permanent shape under 37 °C in a hydrated condition [33]. The shape recovery induced the buckling of PEM thin film to achieve nano-wrinkle formation. To characterize the dynamic change of wrinkle morphology, AFM was used to scan Geltrex-coated SMP-PEM substrate every 15 min after triggering the temperature switch for shape recovery. The time point when SMP-PEM substrate was transferred from 30 °C to 37 °C was noted as 0 min, which showed a flat surface. During shape recovery, SMP-PEM showed gradual wrinkle formation on the surface. At 15 min after temperature triggering, wrinkles had an average depth of ~50 nm and an average width of ~800 nm. The wrinkle width decreased to a stable level of ~600 nm at 30 min after temperature triggering, while the depth increased to a stable level of ~200 nm at 45 min (Fig. 1 b). We also conducted AFM measurements on the SMP-PEM surface at 2, 4, and 6 h post temperature triggering, which further proved there was no obvious topographic change after 45 min (Fig. S2).

To characterize the surface stiffness of the polymer substrates, micro-indentation measurements were performed for three different substrates (SMP only, SMP-PEM Flat, SMP-PEM Wrinkled) (Fig. S3). By conducting 8 measurements on each substrate at different locations, we have the Young's Modulus for different substrates: $E_{Wrinkled} = 2.78 \pm 0.12GPa$, $E_{Flat} = 2.55 \pm 0.09GPa$ and $E_{SMP\ only} = 2.01 \pm 0.08GPa$, which are consistent with the order of magnitude reported in the literature [38]. It was shown that wrinkle substrate was stiffer than flat substrate, which might be related to the intrinsic stiffening caused by the wrinkle formation.

3.2. Focal adhesions of hiPSC-CMs on different substrates

Focal adhesions of hiPSC-CMs on a wrinkled surface were stained by paxillin, vinculin and zyxin, together with myofibril filaments stained by F-actin (Fig. 1 c). The pFAs were located near cell periphery, aggregating at the end of F-actin bundles. Focal adhesions with a repeating pattern that were co-localized with sarcomeres were the costameres of hiPSC-CMs. The images showed that paxillin and vinculin were more abundant in the pFAs, while zyxin was more abundant in the costameres, indicating a closer spatial relationship with myofibrils.

To study how focal adhesions of hiPSC-CMs would respond differently to static and dynamic surfaces, we set up three experimental groups: static unstrained flat surface, static pre-recovered wrinkled surface, and dynamic flat-to-wrinkled surface (Fig. 2 a). To keep the consistency of temperature conditions experienced by the three groups, hiPSC-CMs were seeded on these substrates at room temperature, incubated for 2 days at 30 °C for cell spreading, and then transferred to 37 °C for another 36 h incubation. First, we measured the orientation, length and fluorescent intensity of pFAs near the cell edge. We found that all the focal adhesion proteins (paxillin, vinculin and zyxin) showed high percentile of anisotropic orientation along the wrinkle direction on both dynamic and static wrinkled surface, while random orientation on the static flat surface (Fig. 2 b-d). By measuring *in-situ* expression of pFAs based on the fluorescent intensity of three proteins, we found that zyxin showed highest difference between wrinkled surface and flat surface, followed by vinculin, while no difference was observed from paxillin (Fig. 2 e). Using length of pFA staining as focal adhesion maturity, we found that only zyxin showed significant longer structure on the static wrinkled surfaces, but no difference for paxillin and vinculin (Fig. 2 f). The analysis of pFA indicated that the surface with wrinkle topography, both static pre-recovered substrate and dynamic flat-to-wrinkle substrate, could effectively aligned the pFAs along the wrinkle direction, but nano-topographic feature had more significant impact on the innermost layer of pFAs on focal adhesion expression and maturation.

To examine how costameres of hiPSC-CMs would respond to different substrates, we measured the tFA density, costamere density, costamere-tFA ratio and costamere-sarcomere ratio. By measuring the numeric change of tFAs, we only found that zyxin showed significantly higher tFA density on static substrate than static wrinkled and dynamic substrates, but no difference for paxillin and vinculin (Fig. 3 b). For the other parameters specifically related to the costamere dynamics, we found no significant difference either among three different focal adhesion proteins (paxillin, vinculin and zyxin) or among three different substrates (Fig. 3 c-e). These numeric analyses of cardiomyocyte costameres suggested that costamere structure was not altered significantly by different topographic features.

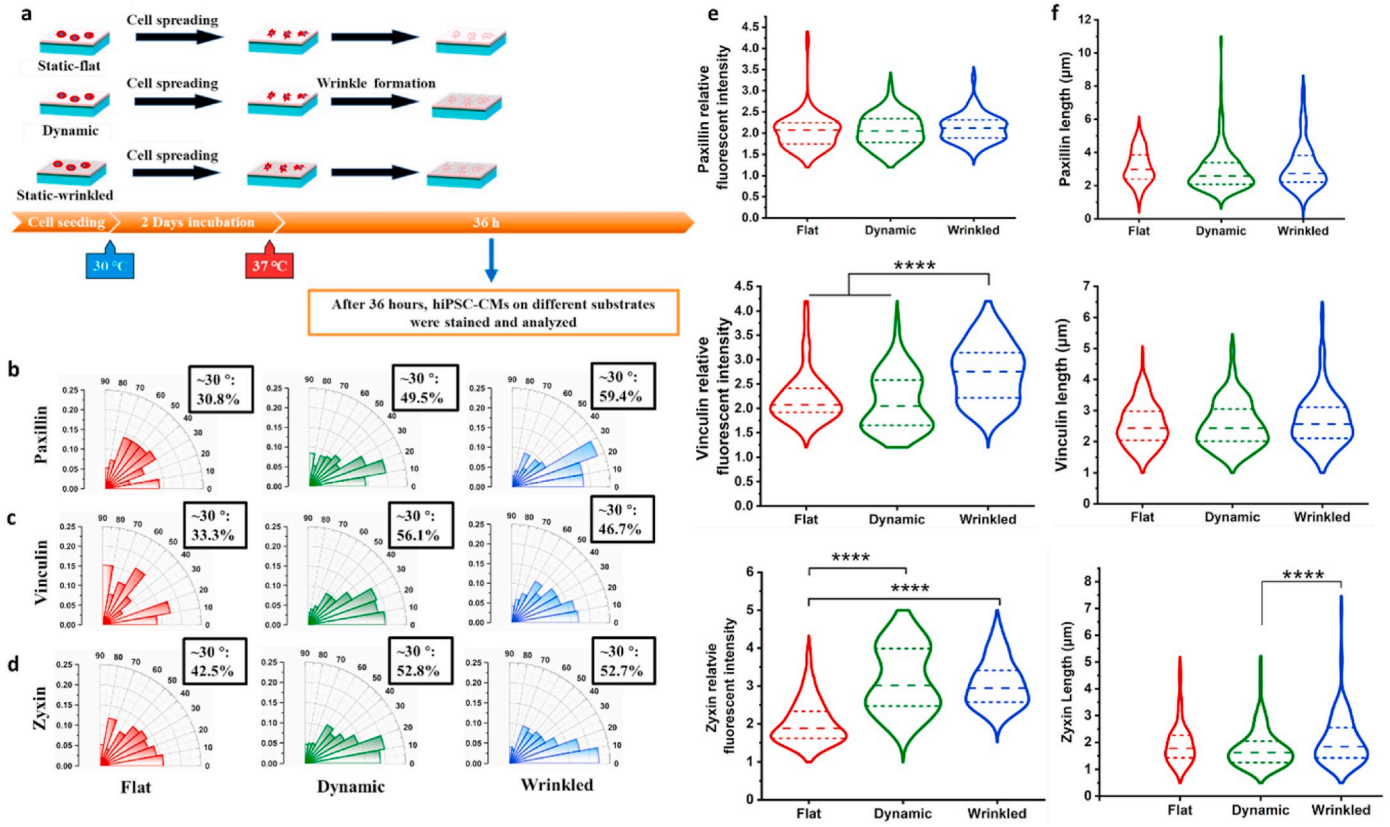

Fig. 2. Responsiveness of pFA of hiPSC-CMs on different substrates. (a) Schematics showing experimental procedures for the investigation of focal adhesions on different substrates. After 2 days spreading under 30 °C, hiPSC-CMs cultured on static flat substrate, dynamic flat-to-wrinkle substrate, and static wrinkled substrate were cultured under 37 °C for another 36 h to investigate how focal adhesions would respond to different substrates. The alignment of pFAs on different substrates was measured by the pFA orientation distribution of (b) paxillin, (c) vinculin, and (d) zyxin. The pFA orientation is defined as the angel between pFA and wrinkle direction. Note boxes demonstrate the percentile of pFA within 30°. The *in-situ* expression of pFAs on different substrates was characterized based on (e) pFA relative fluorescent intensity of paxillin, vinculin and zyxin. The maturation of pFA was measured based on (f) pFA length of paxillin, vinculin and zyxin. Median of each group was labeled by the dash line, while 25% quantile and 75% quantile was labeled by short dash lines in each violin plot. ****$p < 0.0001$.

3.3. Responsiveness of pFAs of hiPSC-CMs to dynamic surface topography

To investigate focal adhesion dynamics, we profiled the responsiveness of focal adhesions of hiPSC-CMs to the topographic changes. Upon triggering the dynamic wrinkle formation via temperature switch as the first time point (Hour 0), samples were collected every hour within next 6 h to analyze both pFAs and costameres. From the orientation distribution of pFAs, we found that the percentile of paxillin and vinculin increased from 30% to over 50% as an anisotropic alignment, which indicated a prominent reorientation of paxillin and vinculin occurring at Hour 3 after triggering wrinkle formation. In contrast, zyxin did not show clear reorientation during the first 6 h in response to the dynamic topographic change (Fig. 4 b-d).

To examine *in-situ* expression of pFAs, we found that fluorescent intensity of paxillin from Hour 1–6 was significantly lower than Hour 0, though the intensity had a clear trend of increase from Hour 3, indicating that the change of extracellular microenvironment induced a fast disassembly and a progressive recovery of outermost layer of pFAs (Fig. 4 e). In reverse to paxillin, fluorescent intensity of vinculin at Hour 2–4 was significantly higher than Hour 0, and then returned to the original level at Hour 6 (Fig. 4 f). This indicated that topographic change increased the mechanical transduction at intermediate layer of focal adhesions right after the wrinkle formation, requiring a temporal upregulation of vinculin. The fluorescent intensity of zyxin showed a similar trend of paxillin of a decrease at early timepoint followed by an increase at later timepoint, as we seen from the previous results that nano-topographic feature had a long-term impact on the innermost layer of pFAs (Fig. 4 g). To examine the maturity of pFAs, we found that length of paxillin showed a similar trend as its fluorescent intensity measurements of early disassembly and then reassembly at later timepoints (Fig. 4 h). Similarly, vinculin length also showed such dynamic pattern of disassembly and reassembly at Hour 3. However, the length of vinculin at Hour 6 was still significantly lower than Hour 0, indicating intermediate layer of pFA was not able to mature within 6 h after dynamic topographic transition (Fig. 4 i). Last, we found that zyxin length was shorter at Hour 3 & 4 in comparison to Hour 5 & 6, indicating a growth and maturation of the innermost layer of focal adhesions without obvious disassembly at earlier hours (Fig. 4 j).

3.4. Responsiveness of costameres of hiPSC-CMs to dynamic surface topography

Clear cardiac costameres were observed from all three focal adhesion proteins (paxillin, vinculin and zyxin) with co-localization of sarcomere structures (Fig. 5 a). First, we found that tFA density showed significant dynamic changes only from vinculin with a higher density at Hour 4–6, which was consistent with previous results of vinculin pFA fluorescent intensity (Fig. 5 b). However, we found no significant difference on costamere density for all three proteins within 6 h post shape recovery triggering, though a slight progress of costameres disassembly-reassembly was observed from vinculin and zyxin (Fig. 5 c). To further illustrate the dynamic relationship between costameres and tFAs, we analyzed the costamere-tFA ratio, which indicates how many focal adhesion sites involve with force transduction through costamere structures. The costamere-tFA ratio showed a decrease trend at early

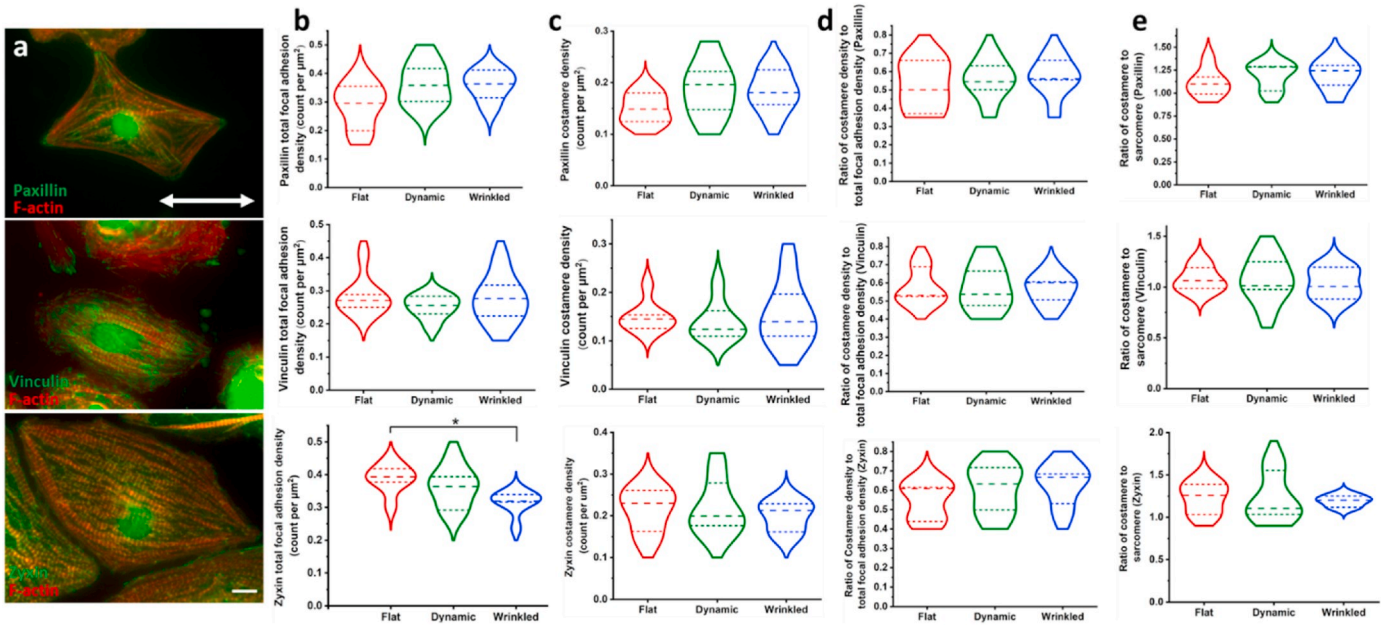

Fig. 3. Characterization of costameres on different substrates. (a) Paxillin, vinculin and zyxin of hiPSC-CMs were co-stained with F-actin showing aligned cell morphology on SMP-PEM substrates (scale bar: 10 μm). Arrow indicates the wrinkle direction. The numeric changes of costameres on different substrates were measured by (b) total tFA density and (c) costamere density of paxillin, vinculin and zyxin. To further characterize how different substrates affect costamere dynamics, we also analyzed (d) costamere-tFA ratio and (e) costamere-sarcomere ratio of paxillin, vinculin and zyxin. Median of each group was labeled by the dash line, while 25% quantile and 75% quantile were labeled by short dash lines in each violin plot. *$p < 0.05$.

timepoints from all three proteins, while zyxin was the first one reaching to the lowest ratio, followed by vinculin and then paxillin. At later timepoints, the costamere-tFA ratio showed an increase trend starting at Hour 4 with paxillin and vinculin, followed by zyxin at Hour 5. These results suggested that the disassembly of costameres followed an inside-out process starting from innermost layer of costameres, while reassembly of costameres followed an outside-in process (Fig. 5 d). Finally, we used the costamere-sarcomere ratio to determine how many sarcomeres anchor to the ECM via costameres. All three proteins showed no significant difference among different timepoints within the first 6 h post shape recovery triggering (Fig. 5 e). Since the costamere structure plays an important role in regulating contractile function of cardiomyocytes, the beating videos of hiPSC-CM contraction were used to analyze contractile functions for hiPSC-CMs on the dynamic substrate with the same timeline of focal adhesion analysis (Movie S1). We found no significant change on beat rate, C-R interval, contraction and relaxation velocity, and X/Y contraction ratio (Fig. S4 b-f), which might be directly related to consistent level of costamere-sarcomere ratio during this 6-h time frame.

Supplementary data related to this article can be found at https://doi.org/10.1016/j.bioactmat.2021.08.028.

4. Discussion

Previous work in the past decades increasingly demonstrated that extracellular mechano-structural cues direct biological responses at both cell and tissue level [39,40]. It was only in recent years, however, that dynamic cell culture platforms based on smart biomaterials have begun to enable in-depth investigations of dynamic cell-matrix mechanobiology [41–43]. With recent advances in stimuli-responsive biomaterials, it is now possible to design and fabricate cytocompatible substrates with dynamic nanoscale properties to investigate how the structural cues of a changing extracellular microenvironment influence cellular development [32,33]. To further enhance our understanding of cardiac dynamic mechanobiology, we employed a biocompatible SMP-PEM substrate, which enabled dynamic topographic transition from a flat surface to a nano-wrinkled surface. Using this dynamic system as cell culture substrate, we successfully profiled the responsiveness of focal adhesions of hiPSC-CMs at initial stages of cellular processes in response to the dynamic change of extracellular microenvironment.

Focal adhesions are assembled upon integrin clusters binding to ECM ligands that further initiate the signaling cascade for stabilization and maturation of focal adhesion complexes [44,45]. Our results suggested that different components of focal adhesion complexes had distinct dynamic profiles in response to the changing extracellular microenvironment. As one of the earliest proteins during focal adhesion assembly, paxillin serves as a structural hub in the outermost layer of focal adhesion architecture and plays an essential role in regulating the focal adhesion turnover [46,47]. In our study, rapid change of surface topography led to a lower affinity of integrin-ECM binding, which caused the disassembly of paxillin pFAs shown as a fast decrease of *in-situ* expression and length at early timepoints (Fig. 4 e,h). Next, focal adhesions re-established based on the surface topographic features starting with paxillin, manifesting as the unidirectional reorientation of paxillin pFA with gradually increased length and intensity from Hour 3.

As the force transducer of focal adhesions, vinculin dynamics are intimately related to the mechanical tension. Recruitment of vinculin could be compromised when the tension is lower than the normal level [48]. We found that vinculin involved in pFAs showed higher fluorescent intensity during Hour 2–5, indicating high expression of vinculin associated with the increase of mechanical signaling from dynamic wrinkle formation. In contrast, reduction of vinculin pFAs length suggested lack of mature pFA formation due to the disassembly of paxillin. Absence of paxillin could alter the spatial distribution of vinculin, which accumulated at force transduction layer and actin regulatory layer of focal adhesions [49]. This indicated that our high expression of vinculin accumulated at force transduction layer and did not form mature pFAs until reassembly of paxillin at the outermost layer (Fig. 4 f). In comparison to the dynamic profile of paxillin pFAs, vinculin dynamics exhibited a time-shift delay in pFA length measurement, indicating a slower recovery for vinculin in mature pFAs (Fig. 4 i).

With a direct binding to the actin filaments, zyxin is critical in maintaining the cytoskeletal integrity [50]. It has been reported that the delocalization of zyxin preceded to both vinculin and paxillin during

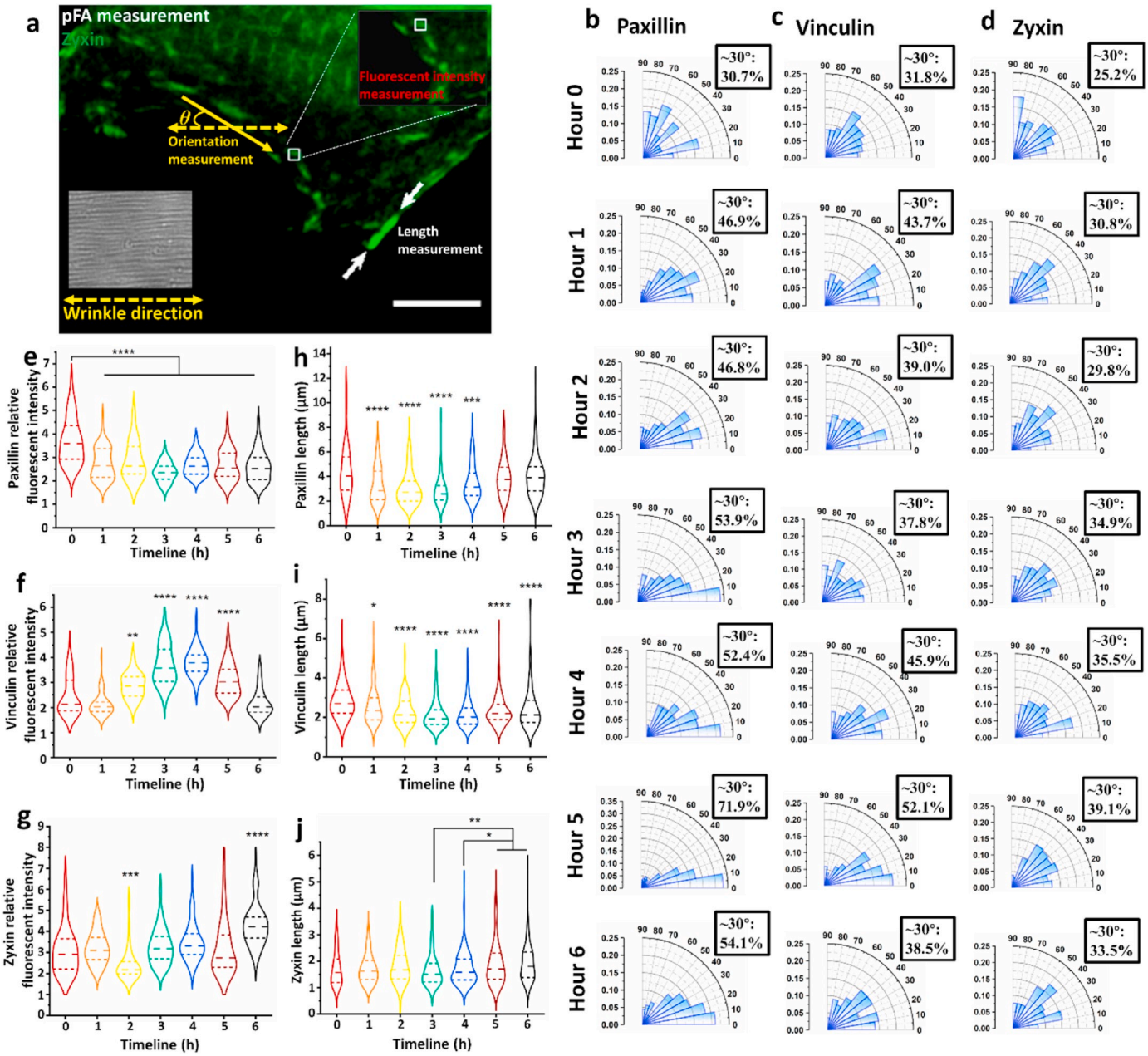

Fig. 4. Responsiveness of hiPSC-CMs' pFA on dynamic SMP-PEM substrate. (a) Fluorescent images of focal adhesions to demonstrate the measurements of pFA orientation, relative fluorescent intensity and length. (scale bar: 8 μm). The pFA orientation distribution of (b) paxillin, (c) vinculin and (d) zyxin in response to dynamic flat-to-wrinkled surface. *In-situ* expression of pFA in response to the dynamic substrate was analyzed by quantifying the relative fluorescent intensity of (e) paxillin, (f) vinculin and (g) zyxin. Matuation of pFAs in response to the dynamic substrate was analyzed by the length measurement of (h) paxillin, (i) vinculin and (j) zyxin. Median of each group was labeled by the dash line, while 25% quantile and 75% quantile was labeled by short dash lines in each violin plot. $^{*}p < 0.05$, $^{**}p < 0.01$, $^{***}p < 0.001$ and $^{****}p < 0.0001$.

focal adhesion disassembly by inhibiting ROCK signaling [51]. However, our results did not indicate an obvious disassembly of zyxin in pFAs in comparison to vinculin and paxillin (Fig. 4 j). We believe that, unlike direct inhibition of myosin contractility, outside-in mechanical signaling from extracellular topographic changes only relocated zyxin from focal adhesions to actin stress fibers [52,53], rather than inducing disassembly of zyxin at focal adhesion sites. Previous studies also showed that actin stress fiber remodeling caused by mechanical signaling was mediated by the recruitment and accumulation of zyxin at focal adhesions [54,55]. This indicated that increased length and intensity of zyxin at pFAs (Fig. 4 g,j) is the prerequisite of actin reinforcement within cardiomyocytes, which may initiate myofibril remodeling and cell morphological change.

The costamere is a striated muscle-specific structure connecting sarcomeres to ECM for force transmission [56,57]. The myofibrillogenesis is initiated when Z-bodies were recruited at immature costamere sites, driven by mechanical loading [58]. Disorganization of non-muscle myosin that disrupts the force transmission could result in costamere deficiency [59]. Similar to pFAs, assembly and maintenance of costameres are also regulated by external mechanical signaling, whereas related research on costamere mechanotransduction is still very limited. Substrate stiffness and static stretching was found to regulate costamere assembly via non-muscle myosin [60–62], though molecular mechanism has not been fully elucidated. Moreover, the responsiveness of costameres to dynamic topographic change is still underexplored. From our study, sharing a similar profile of pFA length results, costamere density

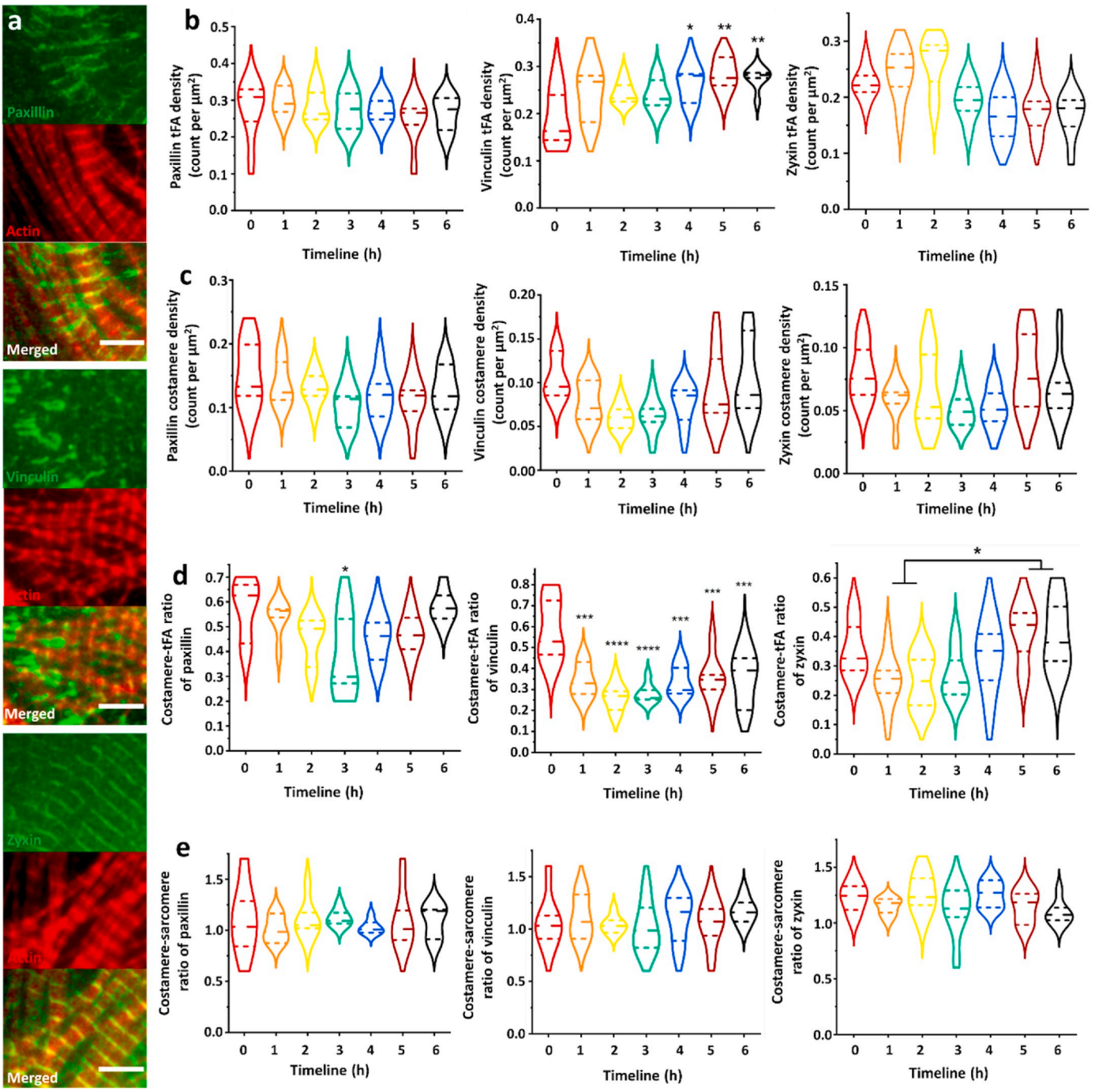

Fig. 5. Responsiveness of hiPSC-CMs' costameres on dynamic SMP-PEM substrate. (a) The fluorescent images of repeating costameres of hiPSC-CMs associating with F-actin (scale bar: 5 μm). The responsiveness of costameres to dynamic substrate was profiled by (b) tFA density, (c) costamere density, (d) costamere-tFA density and (e) costamere-sarcomere ratio of paxillin, vinculin and zyxin. Median of each group was labeled by the dash line, while 25% quantile and 75% quantile was labeled by short dash lines in each violin plot. *$p < 0.05$, **$p < 0.01$, ***$p < 0.001$ and ****$p < 0.0001$.

(Fig. 5 c) and costamere-tFA ratio (Fig. 5 d) decreased at early timepoints and then increased at late timepoints, suggesting that costameres shared similar characteristics as mature focal adhesions. This also suggested that dynamic topographic changes caused unstable cell-ECM binding, triggering the disassembly and reassembly of costameres. Though costameres are tightly related to sarcomere growth and stabilization, we found no significant change on costamere-sarcomere ratio in response to the changing extracellular microenvironment (Fig. 5 e), suggesting that the change of costameres was dynamically correlated to the sarcomere remodeling. The costameres served as a mechanical buffer between extracellular microenvironment and intracellular myofibrils, thus the mechanical input from dynamic surface topography could be absorbed by the costameres to avoid a direct impact on myofibril structure and contractile function.

For our programmable *t*BA-*co*-BA SMP system, we demonstrated that full wrinkle formation can be achieved within 30 min at 42 °C under dry condition, and within 45 min at 37 °C under liquid condition, suggesting that the recovery rate of SMP can be modified with different triggering temperatures. The shape recovery behaviors of thermo-responsive SMP can be affected by the volume fraction of components [63], and more

importantly, by the difference between external triggering temperature and its intrinsic glass transition temperature [64]. The glass transition temperature of this thermo-responsive SMP can be modified by fabricating the SMP with different ratios of *t*BA and BA components, which enables great potentials of this SMP system for various applications that might require different triggering temperatures [65]. In the current study, temperature-based shape changing stimulus is sufficient for investigating the cellular development of human cardiomyocytes, since it is relatively easy to provide biological controls under *in vitro* conditions to rule out the thermal effect on the cells. Despite the *in vitro* applications of SMP, emerging potentials of SMPs in biomedical applications might require more physiologically relevant stimuli to trigger the shape recovery under *in vivo* conditions [66]. It has been reported that the shape recovery behaviors of polyurethane-based SMP can be actuated with ethanol/water treatment under body temperature, which could largely broaden the *in-vivo* feasibility of SMP [67].

5. Conclusions

In this study, we used a SMP-based platform to study how cardiomyocyte focal adhesions would respond to the dynamic nano-topographic cues from extracellular microenvironment. This SMP-PEM system can achieve a flat-to-wrinkle topographic change within 45 min, triggering a dynamic mechanical input to the hiPSC-CMs. In response to dynamic nano-wrinkle formation, focal adhesions of hiPSC-CMs, including pFAs and costameres, demonstrated a pattern of disassembly at early timepoints and reassembly at later timepoints. Proteins from different layers of focal adhesion complexes showed distinct dynamic responsiveness profiles: paxillin (outermost integrin signaling layer) showed the fastest response to the topographic changes, followed by vinculin (force transmission layer), whereas zyxin (innermost actin regulatory layer) did not show an obvious dynamic change. In future, additional characterization on other components of focal adhesion complex (e.g., non-muscle myosin II, desmin, myomesin and talin) in a time-dependent manner will provide more comprehensive evidence for complementing the focal adhesion responsiveness profile.

CRediT authorship contribution statement

Huaiyu Shi: conceived and designed the experiments, performed the polymer sample fabrication and biological experiments, Writing – original draft, with discussions and improvements from all the authors. **Xiangjun Wu:** performed atomic force microscopy. **Shiyang Sun:** developed the experimental procedures of hiPSC-CMs culture on shape memory polymer substrate. **Chenyan Wang:** performed confocal microscopy and hiPSC-CM differentiation. **Zacharias Vangelatos:** performed the mechanical testing experiments. **Ariel Ash-Shakoor:** developed the shape memory polymer system. **Costas P. Grigoropoulos:** supervise mechanical characterization of polymer substrates. **Patrick T. Mather:** developed the shape memory polymer system. **James H. Henderson:** developed the shape memory polymer system. **Zhen Ma:** conceived and designed the experiments, Writing – original draft, with discussions and improvements from all the authors, supervised the project development and funded the study.

Declaration of competing interest

The authors declare no competing financial interest.

Acknowledgement

This work was supported by the NIH NICHD [R01HD101130], NSF [CBET-1804875, CBET-1943798 and CMMI-2130192], NSF [DMR-1609523 and CMMI-2022421] and Syracuse University intramural CUSE Grant, Gerber Grant and BioInspired Institute Seed Grant.

Appendix A. Supplementary data

Supplementary data to this article can be found online at https://doi.org/10.1016/j.bioactmat.2021.08.028.

Data availability

The raw and processed data required to reproduce these findings will be made available via contact with corresponding author Z.M. (zma112@syr.edu).

References

[1] S. Dobbenga, L.E. Fratila-Apachitei, A.A. Zadpoor, Nanopattern-induced osteogenic differentiation of stem cells – a systematic review, Acta Biomater. 46 (2016) 3–14, https://doi.org/10.1016/j.actbio.2016.09.031.
[2] S.F. Badylak, D.O. Freytes, T.W. Gilbert, Extracellular matrix as a biological scaffold material: structure and function, Acta Biomater. 5 (2009) 1–13, https://doi.org/10.1016/j.actbio.2008.09.013.
[3] E.K.F. Yim, M.P. Sheetz, Force-dependent cell signaling in stem cell differentiation, Stem Cell Res. Ther. (2012) 3, https://doi.org/10.1186/scrt132.
[4] A.K. Peter, H. Cheng, R.S. Ross, K.U. Knowlton, J. Chen, Progress in Pediatric Cardiology the costamere bridges sarcomeres to the sarcolemma in striated muscle, Prog. Pediatr. Cardiol. 31 (2011) 83–88, https://doi.org/10.1016/j.ppedcard.2011.02.003.
[5] A. Mihic, J. Li, Y. Miyagi, M. Gagliardi, S.H. Li, J. Zu, R.D. Weisel, G. Keller, R.K. Li, The effect of cyclic stretch on maturation and 3D tissue formation of human embryonic stem cell-derived cardiomyocytes, Biomaterials 35 (2014) 2798–2808, https://doi.org/10.1016/j.biomaterials.2013.12.052.
[6] N.L. Tulloch, V. Muskheli, M.V. Razumova, F.S. Korte, M. Regnier, K.D. Hauch, L. Pabon, H. Reinecke, C.E. Murry, Growth of engineered human myocardium with mechanical loading and vascular coculture, Circ. Res. 109 (2011) 47–59, https://doi.org/10.1161/CIRCRESAHA.110.237206.
[7] N.J. Sniadecki, A. Anguelouch, M.T. Yang, C.M. Lamb, Z. Liu, S.B. Kirschner, Y. Liu, D.H. Reich, C.S. Chen, Magnetic microposts as an approach to apply forces to living cells, Proc. Natl. Acad. Sci. U. S. A. 104 (2007) 14553–14558, https://doi.org/10.1073/pnas.0611613104.
[8] F.X. Jiang, B. Yurke, R.S. Schloss, B.L. Firestein, N.A. Langrana, Effect of dynamic stiffness of the substrates on neurite outgrowth by using a DNA-crosslinked hydrogel, Tissue Eng. 16 (2010) 1873–1889, https://doi.org/10.1089/ten.tea.2009.0574.
[9] A.M. Rosales, K.M. Mabry, E.M. Nehls, K.S. Anseth, Photoresponsive elastic properties of azobenzene-containing poly(ethylene-glycol)-based hydrogels, Biomacromolecules 16 (2015) 798–806, https://doi.org/10.1021/bm501710e.
[10] T. Yang, R. Ji, X.X. Deng, F.S. Du, Z.C. Li, Glucose-responsive hydrogels based on dynamic covalent chemistry and inclusion complexation, Soft Matter 10 (2014) 2671–2678, https://doi.org/10.1039/c3sm53059k.
[11] K.A. Davis, K.A. Burke, P.T. Mather, J.H. Henderson, Dynamic cell behavior on shape memory polymer substrates, Biomaterials 32 (2011) 2285–2293, https://doi.org/10.1016/j.biomaterials.2010.12.006.
[12] C. Rianna, A. Calabuig, M. Ventre, S. Cavalli, V. Pagliarulo, S. Grilli, P. Ferraro, P. A. Netti, Reversible holographic patterns on azopolymers for guiding cell adhesion and orientation, ACS Appl. Mater. Interfaces 7 (2015), https://doi.org/10.1021/acsami.5b02080, 16984–16991.
[13] C. Yang, M.W. Tibbitt, L. Basta, K.S. Anseth, Mechanical memory and dosing influence stem cell fate, Nat. Mater. 13 (2014) 645–652, https://doi.org/10.1038/nmat3889.
[14] T. Gong, K. Zhao, G. Yang, J. Li, H. Chen, Y. Chen, S. Zhou, The control of mesenchymal stem cell differentiation using dynamically tunable surface microgrooves, Advanced Healthcare Materials 3 (2014) 1608–1619, https://doi.org/10.1002/adhm.201300692.
[15] C. Fedele, E. Mäntylä, B. Belardi, T. Hamkins-Indik, S. Cavalli, P.A. Netti, D. A. Fletcher, S. Nymark, A. Priimagi, T.O. Ihalainen, Azobenzene-based sinusoidal surface topography drives focal adhesion confinement and guides collective migration of epithelial cells, Sci. Rep. 10 (2020) 1–15, https://doi.org/10.1038/s41598-020-71567-w.
[16] C.F. Natale, J. Lafaurie-Janvore, M. Ventre, A. Babataheri, A.I. Barakat, Focal adhesion clustering drives endothelial cell morphology on patterned surfaces, J. R. Soc. Interface 16 (2019), https://doi.org/10.1098/rsif.2019.0263.
[17] C. González-García, S.R. Sousa, D. Moratal, P. Rico, M. Salmerón-Sánchez, Effect of nanoscale topography on fibronectin adsorption, focal adhesion size and matrix organisation, Colloids Surf. B Biointerfaces 77 (2010) 181–190, https://doi.org/10.1016/j.colsurfb.2010.01.021.
[18] A.K. Yip, A.T. Nguyen, M. Rizwan, S.T. Wong, K.H. Chiam, E.K.F. Yim, Anisotropic traction stresses and focal adhesion polarization mediates topography-induced cell elongation, Biomaterials 181 (2018) 103–112, https://doi.org/10.1016/j.biomaterials.2018.07.057.
[19] C.H. Seo, H. Jeong, K.S. Furukawa, Y. Suzuki, T. Ushida, The switching of focal adhesion maturation sites and actin filament activation for MSCs by topography of well-defined micropatterned surfaces, Biomaterials 34 (2013) 1764–1771, https://doi.org/10.1016/j.biomaterials.2012.11.031.

[20] P. Kanchanawong, G. Shtengel, A.M. Pasapera, E.B. Ramko, M.W. Davidson, H. F. Hess, C.M. Waterman, Nanoscale architecture of integrin-based cell adhesions, Nature 468 (2010) 580–584, https://doi.org/10.1038/nature09621.

[21] G. Abagnale, M. Steger, V.H. Nguyen, N. Hersch, A. Sechi, S. Joussen, B. Denecke, R. Merkel, B. Hoffmann, A. Dreser, U. Schnakenberg, A. Gillner, W. Wagner, Surface topography enhances differentiation of mesenchymal stem cells towards osteogenic and adipogenic lineages, Biomaterials 61 (2015) 316–326, https://doi.org/10.1016/j.biomaterials.2015.05.030.

[22] J.P. Spatz, B. Geiger, Molecular engineering of cellular environments: cell adhesion to nano-digital surfaces, Methods Cell Biol. 83 (2007) 89–111, https://doi.org/10.1016/S0091-679X(07)83005-6.

[23] M. Arnold, E.A. Cavalcanti-Adam, R. Glass, J. Blümmel, W. Eck, M. Kantlehner, H. Kessler, J.P. Spatz, Activation of integrin function by nanopatterned adhesive interfaces, ChemPhysChem 5 (2004) 383–388, https://doi.org/10.1002/cphc.200301014.

[24] P.Y. Wang, J. Yu, J.H. Lin, W.B. Tsai, Modulation of alignment, elongation and contraction of cardiomyocytes through a combination of nanotopography and rigidity of substrates, Acta Biomater. 7 (2011) 3285–3293, https://doi.org/10.1016/j.actbio.2011.05.021.

[25] D. Motlagh, S.E. Senyo, T.A. Desai, B. Russell, Microtextured substrata alter gene expression, protein localization and the shape of cardiac myocytes, Biomaterials 24 (2003) 2463–2476, https://doi.org/10.1016/S0142-9612(02)00644-0.

[26] N.E. Oyunbaatar, A. Shanmugasundaram, D.W. Lee, Contractile behaviors of cardiac muscle cells on mushroom-shaped micropillar arrays, Colloids Surf. B Biointerfaces 174 (2019) 103–109, https://doi.org/10.1016/j.colsurfb.2018.10.058.

[27] H.T. Heidi Au, B. Cui, Z.E. Chu, T. Veres, M. Radisic, Cell culture chips for simultaneous application of topographical and electrical cues enhance phenotype of cardiomyocytes, Lab Chip 9 (2009) 564–575, https://doi.org/10.1039/b810034a.

[28] C. Cimmino, L. Rossano, P.A. Netti, M. Ventre, Spatio-temporal control of cell adhesion: toward programmable platforms to manipulate cell functions and fate, Frontiers in Bioengineering and Biotechnology 6 (2018), https://doi.org/10.3389/fbioe.2018.00190.

[29] B. Sen, C. Guilluy, Z. Xie, N. Case, M. Styner, J. Thomas, I. Oguz, C. Rubin, K. Burridge, J. Rubin, Mechanically induced focal adhesion assembly amplifies anti-adipogenic pathways in mesenchymal stem cells, Stem Cell. 29 (2011) 1829–1836, https://doi.org/10.1002/stem.732.

[30] A.M. Goldyn, B.A. Rioja, J.P. Spatz, C. Ballestrem, R. Kemkemer, Force-induced cell polarisation is linked to RhoA-driven microtubule-independent focal-adhesion sliding, J. Cell Sci. 122 (2009) 3644–3651, https://doi.org/10.1242/jcs.054866.

[31] J. Lou, R. Stowers, S. Nam, Y. Xia, O. Chaudhuri, Stress relaxing hyaluronic acid-collagen hydrogels promote cell spreading, fiber remodeling, and focal adhesion formation in 3D cell culture, Biomaterials 154 (2018) 213–222, https://doi.org/10.1016/j.biomaterials.2017.11.004.

[32] P.Y. Mengsteab, K. Uto, A.S.T. Smith, S. Frankel, E. Fisher, Z. Nawas, J. Macadangdang, M. Ebara, D.H. Kim, Spatiotemporal control of cardiac anisotropy using dynamic nanotopographic cues, Biomaterials 86 (2016) 1–10, https://doi.org/10.1016/j.biomaterials.2016.01.062.

[33] S. Sun, H. Shi, S. Moore, C. Wang, A. Ash-Shakoor, P.T. Mather, J.H. Henderson, Z. Ma, Progressive myofibril reorganization of human cardiomyocytes on a dynamic nano-topographic substrate, ACS Appl. Mater. Interfaces 12 (2020) 21450–21462, https://doi.org/10.1021/acsami.0c03464.

[34] P. Hoang, J. Wang, B.R. Conklin, K.E. Healy, Z. Ma, Generation of spatial-patterned early-developing cardiac organoids using human pluripotent stem cells, Nat. Protoc. 13 (2018) 723–737, https://doi.org/10.1038/nprot.2018.006.

[35] X. Lian, C. Hsiao, G. Wilson, K. Zhu, L.B. Hazeltine, S.M. Azarin, K.K. Raval, J. Zhang, T.J. Kamp, S.P. Palecek, Robust cardiomyocyte differentiation from human pluripotent stem cells via temporal modulation of canonical Wnt signaling, Proc. Natl. Acad. Sci. U. S. A. 109 (2012) E1848–E1857, https://doi.org/10.1073/pnas.1200250109.

[36] R.M. Delaine-Smith, S. Burney, F.R. Balkwill, M.M. Knight, Experimental validation of a flat punch indentation methodology calibrated against unconfined compression tests for determination of soft tissue biomechanics, Journal of the Mechanical Behavior of Biomedical Materials 60 (2016) 401–415, https://doi.org/10.1016/j.jmbbm.2016.02.019.

[37] W.C. Oliver, G.M. Pharr, An Improved Technique for Determining Hardness and Elastic Modulus Using Load and Displacement Sensing Indentation Experiments, 1992.

[38] E.A. Pieczyska, W.K. Nowacki, H. Tobushi, S. Hayashi, Thermomechanical properties of shape memory polymer subjected to tension in various conditions, Quantitative InfraRed Thermography Journal 6 (2009) 189–205, https://doi.org/10.3166/qirt.6.189-205.

[39] N.V. Bukoreshtliev, K. Haase, A.E. Pelling, Mechanical cues in cellular signalling and communication, Cell Tissue Res. 352 (2013) 77–94, https://doi.org/10.1007/s00441-012-1531-4.

[40] T. Mammoto, D.E. Ingber, Mechanical control of tissue and organ development, Development 137 (2010) 1407–1420, https://doi.org/10.1242/dev.024166.

[41] E.A. Corbin, A. Vite, E.G. Peyster, M. Bhoopalam, J. Brandimarto, X. Wang, A. I. Bennett, A.T. Clark, X. Cheng, K.T. Turner, K. Musunuru, K.B. Margulies, Tunable and reversible substrate stiffness reveals a dynamic mechanosensitivity of cardiomyocytes, ACS Appl. Mater. Interfaces 11 (2019), https://doi.org/10.1021/acsami.9b02446, 20603–20614.

[42] J. Kim, R.C. Hayward, Mimicking dynamic in vivo environments with stimuli-responsive materials for cell culture, Trends Biotechnol. 30 (2012) 426–439, https://doi.org/10.1016/j.tibtech.2012.04.003.

[43] J.L. Young, A.J. Engler, Hydrogels with time-dependent material properties enhance cardiomyocyte differentiation in vitro, Biomaterials 32 (2011) 1002–1009, https://doi.org/10.1016/j.biomaterials.2010.10.020.

[44] O. Rossier, V. Octeau, J.B. Sibarita, C. Leduc, B. Tessier, D. Nair, V. Gatterdam, O. Destaing, C. Albigès-Rizo, R. Tampé, L. Cognet, D. Choquet, B. Lounis, G. Giannone, Integrins β 1 and β 3 exhibit distinct dynamic nanoscale organizations inside focal adhesions, Nat. Cell Biol. 14 (2012) 1057–1067, https://doi.org/10.1038/ncb2588.

[45] A. Banno, B.T. Goult, H.S. Lee, N. Bate, D.R. Critchley, M.H. Ginsberg, Subcellular localization of talin is regulated by inter-domain interactions, J. Biol. Chem. 287 (2012) 13799–13812, https://doi.org/10.1074/jbc.M112.341214.

[46] C.K. Choi, J. Zareno, M.A. Digman, E. Gratton, A.R. Horwitz, Cross-correlated fluctuation analysis reveals phosphorylation-regulated paxillin-fak complexes in nascent adhesions, Biophys. J. 100 (2011) 583–592, https://doi.org/10.1016/j.bpj.2010.12.3719.

[47] D.J. Webb, K. Donais, L.A. Whitmore, S.M. Thomas, C.E. Turner, J.T. Parsons, A. F. Horwitz, FAK-Src signalling through paxillin, ERK and MLCK regulates adhesion disassembly, Nat. Cell Biol. 6 (2004) 154–161, https://doi.org/10.1038/ncb1094.

[48] C. Grashoff, B.D. Hoffman, M.D. Brenner, R. Zhou, M. Parsons, M.T. Yang, M. A. McLean, S.G. Sligar, C.S. Chen, T. Ha, M.A. Schwartz, Measuring mechanical tension across vinculin reveals regulation of focal adhesion dynamics, Nature 466 (2010) 263–266, https://doi.org/10.1038/nature09198.

[49] L.B. Case, M.A. Baird, G. Shtengel, S.L. Campbell, H.F. Hess, M.W. Davidson, C. M. Waterman, Molecular mechanism of vinculin activation and nanoscale spatial organization in focal adhesions, Nat. Cell Biol. 17 (2015) 880–892, https://doi.org/10.1038/ncb3180.

[50] G. Li, X. Song, R. Li, L. Sun, X. Gong, C. Chen, Zyxin - involved actin regulation is essential in the maintenance of vinculin focal adhesion and chondrocyte differentiation status, Cell Prolif 52 (2019), e12532, https://doi.org/10.1111/cpr.12532.

[51] K. Rottner, M. Krause, M. Gimona, J.V. Small, Zyxin is not colocalized with vasodilator-stimulated phosphoprotein (VASP) at lamellipodial tips and exhibits different dynamics to vinculin, Paxillin , and VASP in Focal Adhesions □ 12 (2001) 3103–3113.

[52] M. Yoshigi, L.M. Hoffman, C.C. Jensen, H.J. Yost, M.C. Beckerle, M. Yoshigi, L. M. Hoffman, C.C. Jensen, H.J. Yost, Mechunical force mobilizes adhesions to actin filament cytoskeletal reinforcement, JCB (J. Cell Biol.) 171 (2021) 209–215.

[53] E. Belgardt, T. Steinberg, A. Husari, M. Philipp, D. Hülter-hassler, B. Jung, P. Tomakidi, Force-responsive Zyxin modulation in periodontal ligament cells is regulated by YAP rather than TAZ, Cell. Signal. 72 (2020) 109662, https://doi.org/10.1016/j.cellsig.2020.109662.

[54] H. Hirata, H. Tatsumi, M. Sokabe, Mechanical forces facilitate actin polymerization at focal adhesions in a zyxin-dependent manner, J. Cell Sci. 121 (2008) 2795–2804, https://doi.org/10.1242/jcs.030320.

[55] M.A. Smith, E. Blankman, M.L. Gardel, L. Luettjohann, C.M. Waterman, M. C. Beckerle, A Zyxin-mediated mechanism for actin stress fiber maintenance and repair, Dev. Cell 19 (2010) 365–376, https://doi.org/10.1016/j.devcel.2010.08.008.

[56] B. Sit, D. Gutmann, T. Iskratsch, Costameres, dense plaques and podosomes: the cell matrix adhesions in cardiovascular mechanosensing, J. Muscle Res. Cell Motil. 40 (2019) 197–209, https://doi.org/10.1007/s10974-019-09529-7.

[57] G. Anastasi, G. Cutroneo, R. Gaeta, D. Di Mauro, A. Arco, A. Consolo, G. Santoro, F. Trimarchi, A. Favaloro, Dystrophin-glycoprotein complex and vinculin-talin-integrin system in human adult cardiac muscle, Int. J. Mol. Med. 23 (2009) 149–159, https://doi.org/10.3892/ijmm_00000112.

[58] N.L. Quach, T.A. Rando, Focal adhesion kinase is essential for costamerogenesis in cultured skeletal muscle cells, Dev. Biol. 293 (2006) 38–52, https://doi.org/10.1016/j.ydbio.2005.12.040.

[59] J.L. Myhre, J.A. Hills, F. Jean, D.B. Pilgrim, Unc45b is essential for early myo fi brillogenesis and costamere formation in zebra fi sh, Dev. Biol. 390 (2014) 26–40, https://doi.org/10.1016/j.ydbio.2014.02.022.

[60] P. Pandey, W. Hawkes, J. Hu, J. Hone, M. Sheetz, T. Iskratsch, P. Pandey, W. Hawkes, J. Hu, W.V. Megone, J. Gautrot, N. Anilkumar, Cardiomyocytes sense matrix rigidity through a combination of muscle and non-muscle myosin article cardiomyocytes sense matrix rigidity through a combination of muscle and non-muscle myosin contractions, Dev. Cell 44 (2018) 326–336, https://doi.org/10.1016/j.devcel.2017.12.024.

[61] P.A. Galie, N. Khalid, K.E. Carnahan, M.V. Westfall, J.P. Stegemann, Substrate stiffness affects sarcomere and costamere structure and electrophysiological function of isolated adult cardiomyocytes, Cardiovasc. Pathol. 22 (2013) 219–227, https://doi.org/10.1016/j.carpath.2012.10.003.

[62] W.W. Shakp, D.G. Simpson, T.K. Borg, A.M. Samarel, L. Terracio, Mechanical forces regulate focal adhesion and costamere assembly in cardiac myocytes, Am. J. Physiol. Heart Circ. Physiol. 273 (1997), https://doi.org/10.1152/ajpheart.1997.273.2.h546.

[63] H. Lu, W.M. Huang, On the origin of the Vogel-Fulcher-Tammann law in the thermo-responsive shape memory effect of amorphous polymers, Smart Mater. Struct. 22 (2013), https://doi.org/10.1088/0964-1726/22/10/105021.

[64] W.M. Huang, B. Yang, L. An, C. Li, Y.S. Chan, Water-driven programmable polyurethane shape memory polymer: demonstration and mechanism, Appl. Phys. Lett. 86 (2005) 1–3, https://doi.org/10.1063/1.1880448.

[65] P. Yang, R.M. Baker, J.H. Henderson, P.T. Mather, In vitro wrinkle formation via shape memory dynamically aligns adherent cells, Soft Matter 9 (2013) 4705–4714, https://doi.org/10.1039/c3sm00024a.
[66] Y.Q. Fu, W.M. Huang, J.K. Luo, H. Lu, Polyurethane shape-memory polymers for biomedical applications. Shape Memory Polymers for Biomedical Applications, Elsevier Ltd, 2015, pp. 167–195, https://doi.org/10.1016/B978-0-85709-698-2.00009-X.
[67] H. Lu, W.M. Huang, Y.Q. Fu, J. Leng, Quantitative separation of the influence of hydrogen bonding of ethanol/water mixture on the shape recovery behavior of polyurethane shape memory polymer, Smart Mater. Struct. 23 (2014), https://doi.org/10.1088/0964-1726/23/12/125041.